Generalized ray tracing method for the calculation of the peripheral refraction induced by an ophthalmic lens

Pilar Rojo
Santiago Royo
Jesus Caum
Jorge Ramírez
Ines Madariaga

SPIE.

Generalized ray tracing method for the calculation of the peripheral refraction induced by an ophthalmic lens

Pilar Rojo,[a,b,*] Santiago Royo,[a] Jesus Caum,[a] Jorge Ramírez,[c] and Ines Madariaga[c]
aUPC-CD6, Center for Sensor, Instruments and Systems Development, Universitat Politècnica de Catalunya, Rambla Sant Nebridi 10, Terrassa E08222, Spain
bClínica Badia. C/Barcelona, 12, 3°, Mataró, E08301, Spain
cIndustrias de Óptica Prats, Dr Josep Castells, 4, S. Boi de Llobregat, E08830, Spain

Abstract. Peripheral refraction, the refractive error present outside the main direction of gaze, has lately attracted interest due to its alleged relationship with the progression of myopia. The ray tracing procedures involved in its calculation need to follow an approach different from those used in conventional ophthalmic lens design, where refractive errors are compensated only in the main direction of gaze. We present a methodology for the evaluation of the peripheral refractive error in ophthalmic lenses, adapting the conventional generalized ray tracing approach to the requirements of the evaluation of peripheral refraction. The nodal point of the eye and a retinal conjugate surface will be used to evaluate the three-dimensional distribution of refractive error around the fovea. The proposed approach enables us to calculate the three-dimensional peripheral refraction induced by any ophthalmic lens at any direction of gaze and to personalize the lens design to the requirements of the user. The complete evaluation process for a given user prescribed with a −5.76D ophthalmic lens for foveal vision is detailed, and comparative results obtained when the geometry of the lens is modified and when the central refractive error is over- or undercorrected. The methodology is also applied for an emmetropic eye to show its application for refractive errors other than myopia. © *The Authors. Published by SPIE under a Creative Commons Attribution 3.0 Unported License. Distribution or reproduction of this work in whole or in part requires full attribution of the original publication, including its DOI.* [DOI: 10.1117/1.OE.54.2.025106]

Keywords: ophthalmic lens design; ophthalmic optics; myopia; peripheral refraction; generalized ray tracing.

Paper 141625 received Oct. 21, 2014; accepted for publication Jan. 8, 2015; published online Feb. 9, 2015.

1 Introduction

In recent years, peripheral refraction has gained relevance due to its potential relationship with the emmetropization process and the development and progression of myopia. It has been proposed that a relative hyperopic refractive error may be a risk factor in starting and further developing myopia.[1–5] This hypothesis supposes that if the image outside the visual axis is hyperopic with respect to the peripheral retina, the growth of the eye will be accelerated to match the optical image with the peripheral retina, which will increase the axial length of the eye, causing peripheral emmetropia and also foveal myopia. However, some studies also have found that relative peripheral refraction does not have a consistent effect on the risk of myopia onset,[6–8] and it has been proposed that the development of peripheral hyperopia seems to be a consequence, rather than a cause, of myopia.

Although the basic hypothesis that a relatively hyperopic peripheral refractive error can lead to the development of human myopia remains the subject of active discussion, the available data support the possibility of an interaction between the states of focus on the axis and in the periphery. Thibos et al.[9] in a more recent study suggest that hyperopic blur is a risk factor only when the eye has a negative spherical aberration, because that is the combination leading to relatively low contrast in the defocused retinal image.

Different methods have been proposed to measure the peripheral refraction of the eye, including subjective refraction, retinoscopy, manual optometers, the double-pass technique, photorefraction, and wavefront sensors, among others[10] In recent years, faster instruments requiring no off-axis fixation, instrument rotation, or numerous realignments across one meridian have been proposed.[11–14] One major advantage of these new instruments is their speed in measuring peripheral refraction, and since they are based on the Hartmann-Shack principle, they are able to assess both refractive errors and higher-order ocular aberrations across the visual field.

Using different techniques, several studies have reported differences in the peripheral refraction patterns of emmetropes, hypermetropes, and myopes.[15–19] Measurements of peripheral refractive error show a strong dependence on the type of visual pattern of the user: while a myopic eye, in general, shows a hyperopic shift relative to the fovea, hypermetropic and emmetropic eyes tend to present a relative myopic shift.

Both the optics of the eye and the shape of the retina are equally influential in peripheral refraction. To take this into account, some authors have fitted nonrotationally symmetrical ellipsoids to retinal surfaces for emmetropic and myopic eyes after magnetic resonance imaging measurements.[19] In general, results show that no symmetry of revolution may be assumed for the retinal surface, and all studies highlight the difficulty of establishing a pattern, or even a common model, for peripheral refraction, because of the great variability present among individuals, even among those who have the same central refractive error.

Besides, ophthalmic lenses are thought to be a key aspect in the progression of myopia, as far as they are the most

*Address all correspondence to: Pilar Rojo, E-mail: pilar.rojo.badenas@gmail.com

common method used in the compensation of myopic children. Children are obviously the population where actions on eye growth in order to prevent the progression of myopia may have more significant effects. Traditional ophthalmic lenses are designed to provide perfect foveal vision for all directions of gaze, but their effect on peripheral refraction has not been taken into account until very recently.[20–23]

Furthermore, some studies have analyzed the effect of ophthalmic lenses on peripheral refraction, that is, the lens-induced peripheral refraction (IPR), and they have been related to an increase in hyperopic defocus. In particular, single vision lenses have been shown to increase the amount of hyperopic blur in eyes with moderate myopia,[24,25] thus contributing to the progression of myopia. It has also been shown that IPR may be manipulated by altering the form of ophthalmic lenses.[26] However, the proposed design methods have been limited to the use of third-order theory to determine off-axis power errors of thin ophthalmic lenses by tracing paraxial chief rays through an effective stop situated at the entrance pupil of the eye and applying the classical Coddington's equations to these chief rays.

Due to the relevance of the topic, a generalized approach for the calculation of the IPR of a given ophthalmic lens would be desirable. The method should ideally be aligned with the common procedures of modern ophthalmic lens design, based on generalized ray tracing (GRT) techniques,[27] in order to yield three-dimensional (3-D) power error maps in the peripheral field of vision of different lens geometries. GRT is a general procedure that goes beyond third-order theory, delivering exact ray tracing in 3-D. The GRT approach enables us, in foveal vision, to reduce the effects of the eye as an optical system to one convenient point (the center of rotation of the eye) and surface (the remote surface). GRT is also the general approach conventionally used in ophthalmic lens design as it is better suited to the ophthalmic lens design problem than conventional software packages. While in ophthalmic lens design a single surface needs to be optimized to yield a proper performance of the lens, even changing its curvature locally to deliver free-form shapes, optical design packages provide a very practical tool to analyze the effects of the lens but are built for optimizing the response of a combination of lenses. Most lens manufacturers optimize their ophthalmic lenses based on GRT algorithms. To properly calculate the IPR, it would also be desirable to analyze the effects on the complete retinal surface and to customize the peripheral refraction to each subject, so that unavoidable intersubject variability is accounted for.

Such a GRT approach for the evaluation of the IPR is proposed in this paper. In the following sections, three consecutive steps of the method will be described in detail using a particular IPR case as a guiding example. First, a methodology for the modeling of a retinal conjugate surface (RCS) from the measured values of peripheral refraction will be presented. Next, a modification of GRT procedures will enable the calculation of the peripheral power error induced by the lens in different retinal eccentricities around the fovea substituting the optics of the eye for a convenient point (the nodal point) and surface (the mentioned RCS). Finally, out of the combination of both procedures, a third subsection describing the calculation of the IPR induced by a particular lens design will be developed. An additional section showing the effects on IPR of changes in the base curve and the asphericity of the lens surface and the effects of under- or overcorrection of the central refractive error will be presented. Following the same trend, an RCS for emmetropes is modeled, and the effects of over- and undercorrection are also discussed. A final section will provide an overview of the main conclusions of the paper.

2 Methodology

2.1 Modeling a Retinal Conjugate Surface

The IPR distribution is dependent on both the optical system of the eye and the retinal surface shape. Thus, it is necessary to define a surface (which we will call the RCS, although it is not physically placed at the retina) defined by the peripheral power error of the subject at different eccentricities around the fovea before the introduction of the lens. As mentioned, different studies suggest it is very difficult to obtain a common pattern for peripheral refraction for myopic eyes due to the considerable individual variability observed. Such RCS could be either modeled on the general shape of some theoretical surface shape (usually rotationally symmetrical surfaces are used, like ellipsoids or hyperboloids)[19] to build a geometrical model of the distribution of refraction at the retina. Alternatively, it may be measured on the subject with some of the techniques discussed above.[10–14] Both methods are equally valid and methodologically equivalent regarding the procedure for evaluation of the IPR. While the first is more general, the second one introduces the measurement accuracy issue, but also the possibility of customization of the ophthalmic lens to the patient. In this paper, we choose to model an experimental RCS out of experimental peripheral refraction data.

Assume that different measurements for peripheral refraction at different angles of eccentricity have been taken in terms of sphere, cylinder, and axis (S, C, θ). Discrete points on different meridians will thus be obtained. Ideally, horizontal, vertical, and some oblique meridians will be measured. Those values of refraction may then be expressed in component vectors $(M, J_0, \text{ and } J_{45})$[28] as follows:

$$M = S + \frac{C}{2}, \tag{1}$$

$$J_0 = -\frac{C}{2} \cos 2\theta, \tag{2}$$

$$J_{45} = -\frac{C}{2} \sin 2\theta, \tag{3}$$

where M stands for the spherical equivalent, J_0 for the power of one cross-cylinder oriented with its axis at 0 deg, and J_{45} for one cross-cylinder oriented with its axis at 45 deg. Any combination of sphere and cylinder can be expressed in terms of M, J_0, and J_{45} using simple algebraic expressions and, conversely, given that all parameters are measured in diopters.

Using these data, a surface may be fitted in terms of M, J_0, and J_{45} to the experimental refraction values by different techniques. An RCS is, thus, obtained in terms of M, J_0, and J_{45}. For the theoretical surface case, the corresponding maps

of M, J_0, and J_{45} would have been directly computed based on the selected geometry of the retina.

As an example, we have used some experimental results obtained from the literature[29] as initial data. Peripheral refraction at different eccentricities (10, 20, and 30 deg) for vertical, horizontal, and oblique meridians for myopic eyes was measured using the ShinNippon autorefractor, one of the commercial instruments most frequently used for peripheral refraction measurements, although it is an instrument not specifically designed for these measurements. However, the data obtained are useful for our purpose because it is primarily used to demonstrate the method introduced and because it is obtained in four meridians covering the full extent of the visual field.

Obviously, this measurement approach does not consider high-order aberrations which degrade optical quality and are not taken into account in this data. It needs to be stressed here that the role of higher-order aberrations remains the subject of discussion, although some authors have pointed out found that the progression of axial myopia in children is not linked to higher-order aberrations.[30,31]

Thus, the mean values of these data will be used to calculate our RCS. For completeness, the values we have used to calculate the RCS are listed in Table 1.

The independent experimental values presented are then fitted to a surface for each of the three parameters. The fit surfaces and their corresponding contour plots are presented in Fig. 1 and will be used as RCS in the following. For referencing purposes, an imaginary plane is set with vertical and horizontal dimensions of ± 15 mm and its origin at the optical axis. This plane is situated 12 mm in front of the anterior corneal surface for convenience, as it will be the position of the back vertex of the ophthalmic lens used in the next section.

Figure 1 shows the results for M, J_0, and J_{45} as 3-D and contour plots based on fitting the data presented in Table 1, using the plane just described.

2.2 Generalized Ray Tracing Applied to the Evaluation of Peripheral Refraction

GRT is now the standard for modern ophthalmic lens design, and its principles and implementation may be found elsewhere.[27] In GRT, a pencil of light can be considered to be composed of a principal ray and a wavefront in its neighborhood. The propagation of the wavefront in the neighborhood of the principal ray through the lens-eye system is used for the evaluation of the performance of the lens.[32,33] GRT allows an exact calculation of the values of oblique astigmatism (OA) in all directions of gaze, and a faster performance than conventional, intensive ray tracing approaches based on general-purpose optical design packages, due to the suitability of the GRT approach to the peculiarities of the ophthalmic lens design problem, where, typically, only one surface of arbitrary shape needs to be optimized.

When lenses are designed for foveal vision, its behavior is calculated by tracing rays through the center of rotation of the eye, a convenient point that enables us to build a remote

Table 1 Mean values of peripheral refraction for myopic eyes used to build the retinal conjugate surface (RCS).[29]

	Temporal retina			Central	Nasal retina		
	−30 deg	−20 deg	−10 deg	0	+10 deg	+20 deg	+30 deg
	Horizontal meridian						
M	−3.71 ± 2.09	−4.97 ± 1.78	−5.62 ± 1.84	−5.76 ± 1.82	−5.54 ± 1.96	−4.96 ± 2.43	−3.69 ± 2.89
J_0	0.14 ± 0.94	−0.05 ± 0.39	0.07 ± 0.18	0.17 ± 0.16	0.23 ± 0.30	0.23 ± 0.33	0.47 ± 0.59
J_{45}	0.31 ± 0.64	0.13 ± 0.40	0.10 ± 0.26	0.04 ± 0.14	−0.01 ± 0.30	−0.02 ± 0.34	−0.01 ± 0.65
	Vertical meridian						
M	−3.32 ± 3.10	−4.96 ± 2.32	−5.50 ± 1.83	−5.76 ± 1.82	−5.56 ± 1.91	−5.22 ± 2.12	−4.36 ± 2.68
J_0	−0.21 ± 1.29	0.16 ± 0.68	0.27 ± 0.45	0.17 ± 0.16	0.26 ± 0.24	0.40 ± 0.37	0.71 ± 0.82
J_{45}	−0.09 ± 0.67	−0.12 ± 0.35	0.01 ± 0.30	0.04 ± 0.14	0.09 ± 0.25	0.21 ± 0.33	0.45 ± 0.58
	Oblique meridian: superior temporal-inferior nasal						
M	−4.47 ± 2.34	−5.11 ± 2.06	−5.63 ± 1.87	−5.76 ± 1.82	−5.71 ± 2.08	−5.18 ± 2.32	−3.85 ± 2.79
J_0	0.28 ± 0.72	0.21 ± 0.35	0.14 ± 0.23	0.17 ± 0.16	0.21 ± 0.32	0.26 ± 0.41	0.11 ± 0.59
J_{45}	0.51 ± 0.94	0.19 ± 0.46	0.18 ± 0.26	0.04 ± 0.14	−0.09 ± 0.24	0.09 ± 0.41	−0.27 ± 0.70
	Oblique meridian: superior nasal-inferior temporal						
M	−3.95 ± 2.96	−4.89 ± 2.37	−5.40 ± 2.17	−5.76 ± 1.82	−5.81 ± 1.95	−5.03 ± 2.05	−3.94 ± 2.11
J_0	0.62 ± 0.51	0.43 ± 0.40	0.21 ± 0.29	0.17 ± 0.16	0.02 ± 0.28	−0.05 ± 0.51	−0.21 ± 0.69
J_{45}	−0.11 ± 0.69	0.00 ± 0.38	−0.03 ± 0.21	0.04 ± 0.14	0.02 ± 0.21	−0.01 ± 0.53	−0.14 ± 0.94
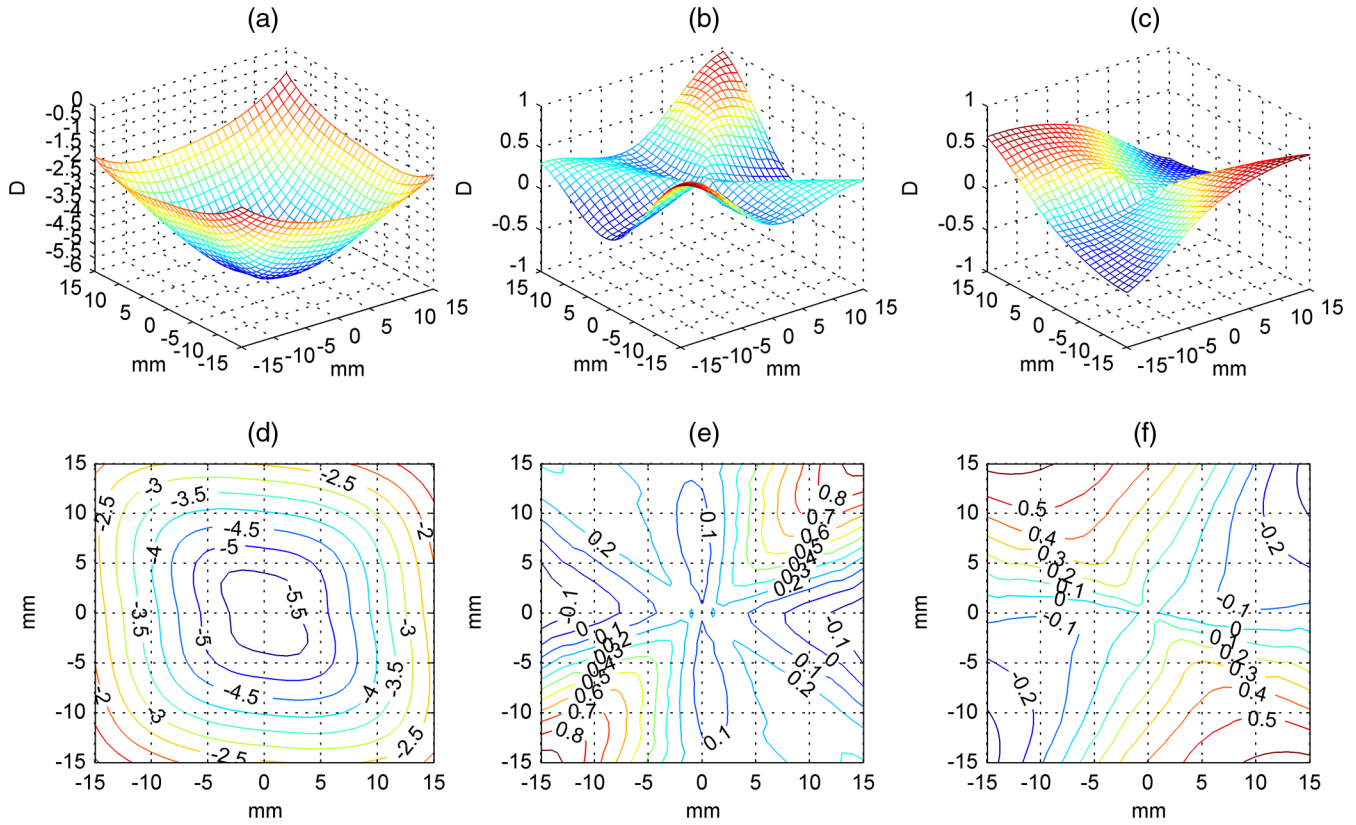
Fig. 1 Retinal conjugate surface (RCS) for M, J_0, and J_{45} using the data from Table 1. Top, surfaces for M (a), J_0 (b), and J_{45} (c); bottom, contour values for the respective surfaces: M (d), J_0 (e), and J_{45} (f).
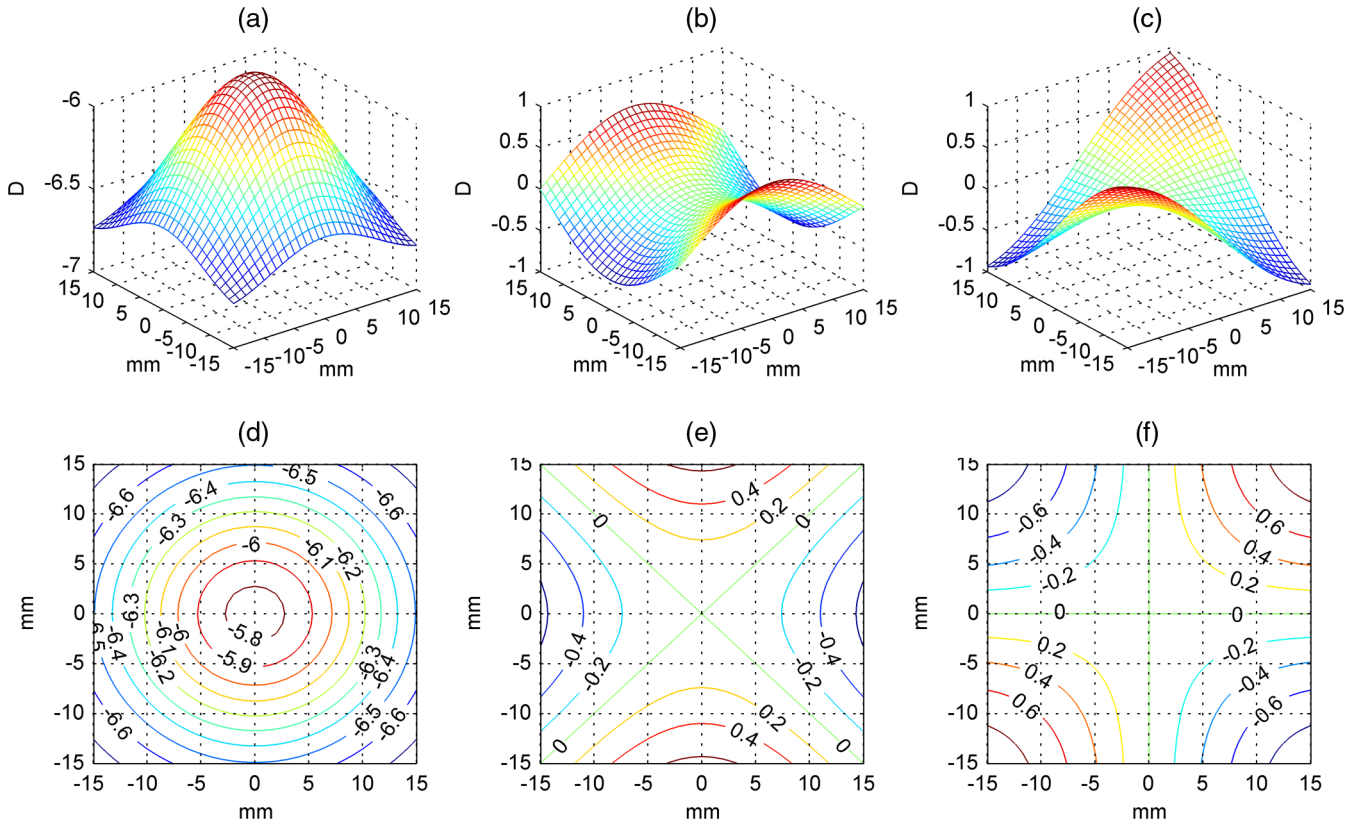
Fig. 2 Peripheral refracted surfaces for M (a), J_0 (b), and J_{45} (c), and contours for M (d), J_0 (e), and J_{45} (f) for a spherical ophthalmic lens with back vertex power (BVP) of −5.76D described in the text. M shows an increase in myopic refraction when eccentricity increases.

sphere, a surface where all remote points of the eye (object points whose image is the fovea) for all directions of gaze are present. This removes the optical elements of the eye from the lens design problem, while enabling a full-field evaluation of the performance of the lens. For peripheral vision, however, the approach needs to be different, as now the point of interest is the behavior of the lens at a fixed retinal eccentricity around the main direction of gaze, which is around the fovea and not at the fovea.

The nodal point of the eye has convenient optical properties which enable the evaluation of the performance of the lens in all eccentricities around the main direction of gaze, as by definition, all rays impinging it are not deviated, becoming the equivalent of the center of rotation of the eye in our ray tracing model. When paraxial models of the eye are considered, the nodal object and image points are seen to be very close to each other, separated by a value of ∼0.3 mm depending on the eye model considered,[34,35] so for our purposes, they can be merged into a single one.[36] The eye will, thus, be assumed to present a single nodal point (combining object and image nodal points, and referred to as nodal point in the following) where traced rays travel from object to image space without deviation. We will use this property of the nodal point to calculate the rays traveling in a given direction around the main direction of gaze, so we may know where they impinge onto the retina.

GRT allows the calculation of the geometry of the refracted wavefront associated with each ray. This geometry is determined by the principal curvatures and directions of the wavefront, which give information on the position of the tangential and sagittal foci and axis, and of the induced OA. Using the conventional GRT algorithms used in ophthalmic lens design through the nodal point of the eye, the tangential and sagittal foci in different eccentric points of the lens outside the main direction of gaze are obtained, which correspond to different eccentricities around the fovea. These values may also be expressed in terms of power vectors, M, J_0, and J_{45}.

For the evaluation of the performance of the ophthalmic lens, a matrix of principal rays with its associated local wavefronts is sent to it and the distribution of OA obtained. Such distribution is then expressed as three surfaces containing the values of parameters M, J_0, and J_{45}[28] at all retinal eccentricities.

Figure 2 shows the peripheral refracted surfaces obtained using this procedure when we consider a spherical lens, which compensates the foveal refractive error of the eye described in Table 1. We calculated a back vertex power (BVP) of −5.76D, with the radius of the convex surface as 298 mm, radius of the concave surface as 76.9 mm, thickness as 1.6 mm, and refractive index as 1.597. The lens is situated 12 mm in front of the anterior corneal surface. The nodal point of the eye is assumed to be 7 mm behind the anterior corneal surface.[36] For referencing purposes, the imaginary plane described above is set at the vertex of the concave surface of the lens, in order to quantify the angular distribution of the rays on the retinal surface. A given retinal eccentricity will then be defined by a ray that crosses
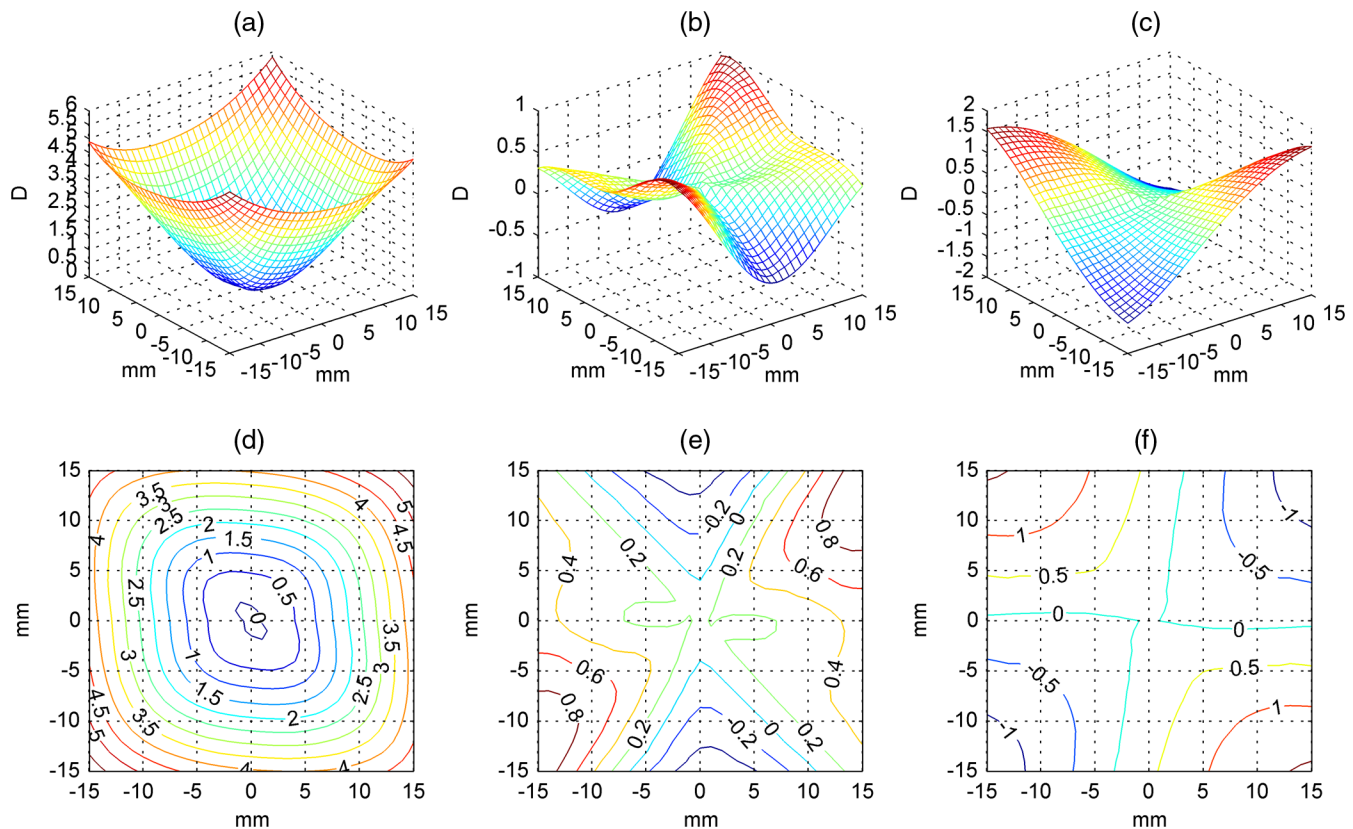
Fig. 3 Lens-induced peripheral refraction (IPR) of the analyzed case for M, J_0, and J_{45}, using the RCS of Fig. 1 and the peripheral refracted surfaces described in Fig. 2. Top, surfaces for M (a), J_0 (b), and J_{45} (c). Bottom, corresponding contour plots for these surfaces [(d), (e), and (f)].

a point (x, y) of this plane and the nodal point. This plane accounts for retinal eccentricities over ± 40 deg around the main direction of gaze, both horizontally and vertically.

As known from ophthalmic lens design theory, such surfaces will be modified when geometrical parameters of the lens change, so a lens with the same BVP but with different base curves, or including an aspheric surface, will produce different peripheral refracted surfaces due to local changes in the OA distribution.

2.3 Calculation of the IPR

Once the RCS and the peripheral refracted surface induced by the ophthalmic lens are both expressed in terms of M, J_0, and J_{45}, the calculation of the IPR is straightforward as it is the local sum of their values. Figure 3 presents the IPR surfaces resulting from the combination of the RCS described in Fig. 1 and the peripheral refracted surface presented in Fig. 2. It can be observed how M, J_0 and J_{45} are compensated in the optical axis but M describes a hyperopia that increases when retinal eccentricity increases. The OA values of J_0 and J_{45} are also presented.

Finally, Fig. 4 shows the results of IPR obtained in Fig. 3 in terms of sphere, cylinder, and axis using Eqs. (1)–(3). The upper plot shows the peripheral distribution of sphere and cylinder as 3-D plots, while the lower plots present it as a contour plot. The cylinder plots include the direction of the axis. It may be appreciated how a nearly zero central

refractive error rises gradually up to 6.00D at the edge of the considered plane.

3 Results

Using the proposed approach, simple but indicative effects on IPR obtained when modifying the geometry of the lens surfaces are easily obtained. In all cases, the RCS presented in Fig. 1 was used. Figures 5 and 6 show the equivalent of Figs. 3 and 4 when the central refractive error is compensated using a lens with BVP of -5.76D but with a base curve of $+8.00$D. This results in a better IPR value for the considered direction of gaze, as can be observed in Fig. 6.

It can be observed how the induced sphere significantly decreases when the base curve increases in this case, so peripheral refraction becomes less hyperopic and, thus (according to the hypothesis of some authors), better suited to avoid the progression of myopia. By iterating this calculation for different base curves, it may be observed how an increase in the curvature of the convex surface decreases the mean sphere in IPR (Fig. 7), showing the potential for an optimization of the curvature to minimize the value of IPR and its effects in the progression of myopia. The induced sphere is presented as a single value calculated as the quadratic sum of all rays evaluated and normalized by the number of rays.

Figure 8 presents the changes in IPR when the concave lens surface becomes aspherical. The performance of the lens
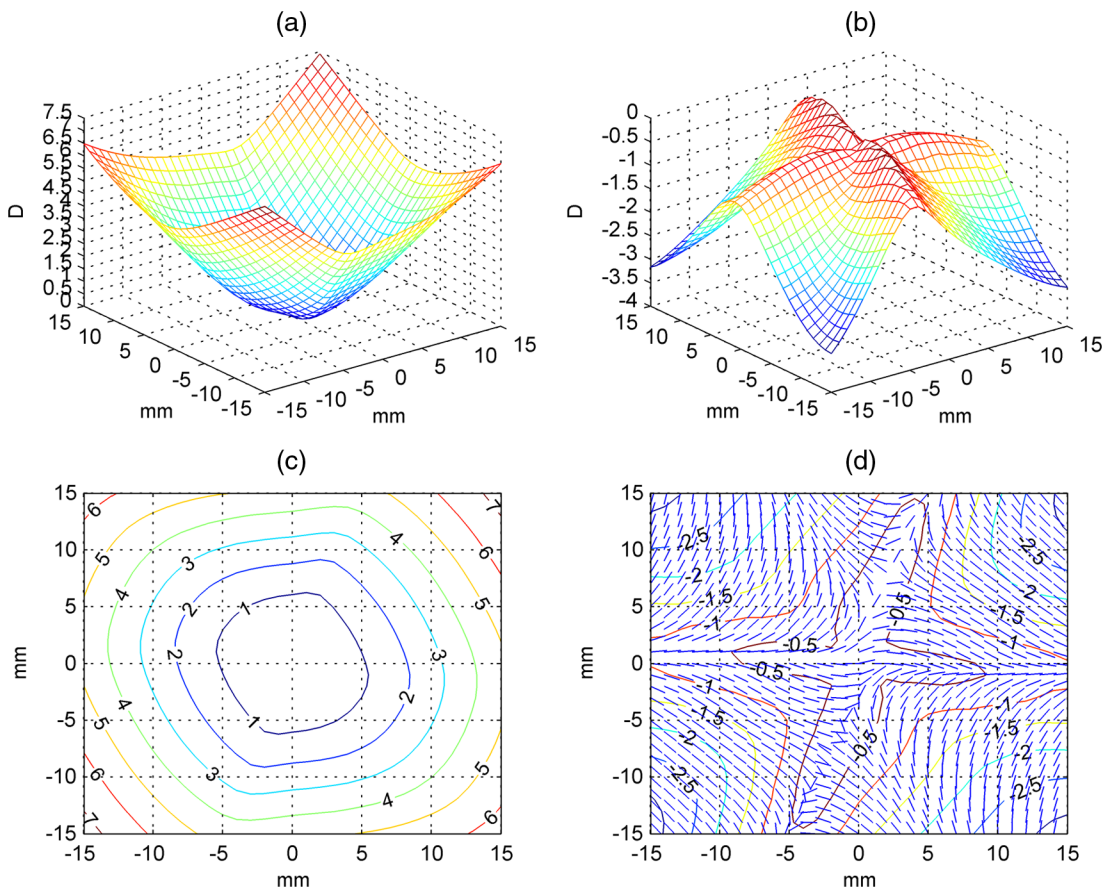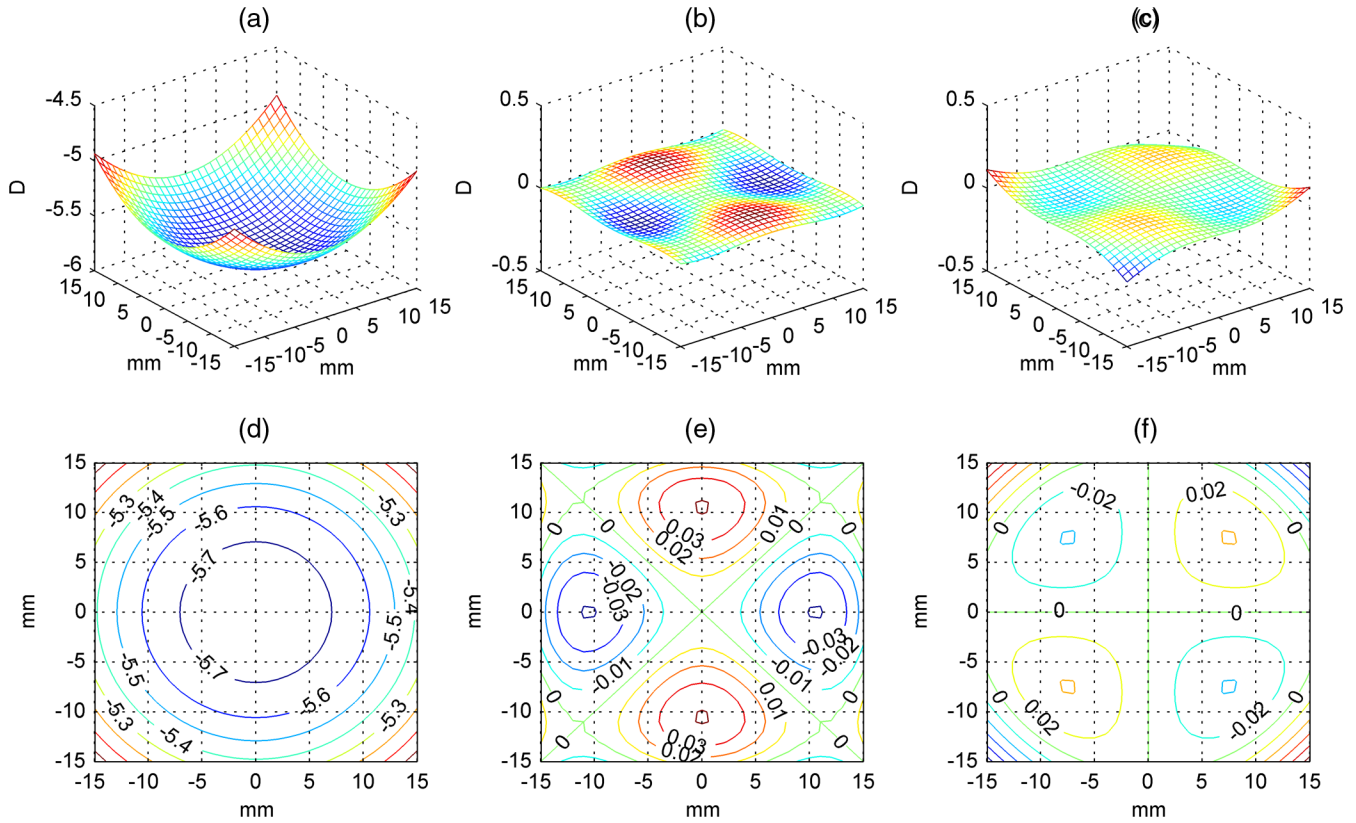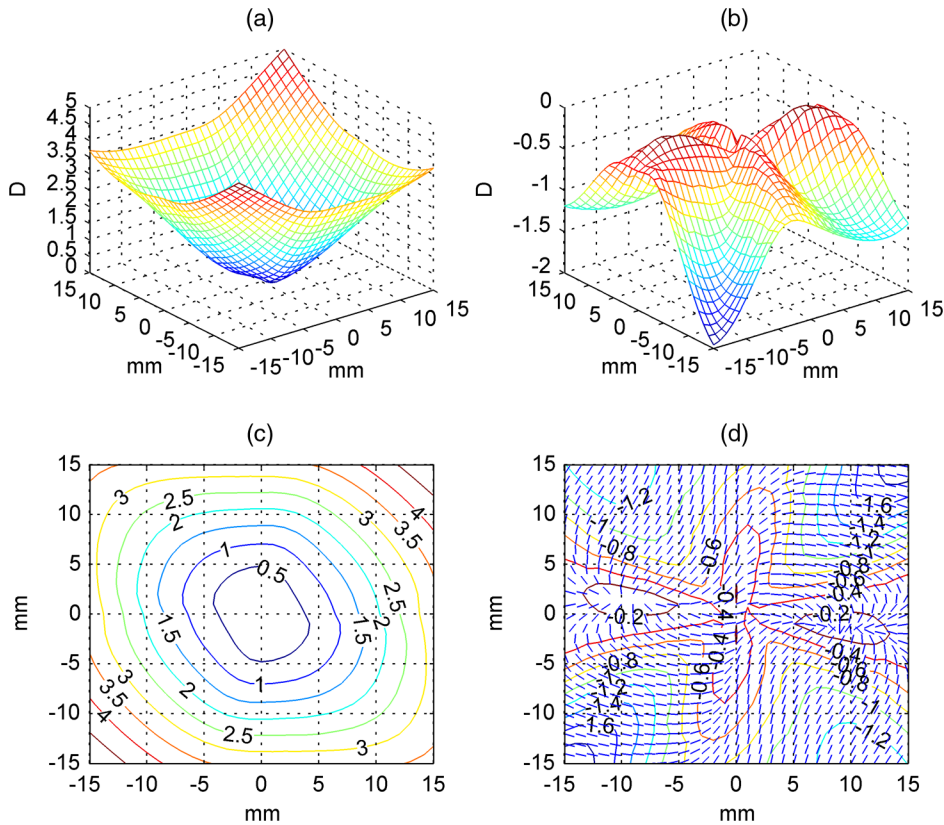

Fig. 4 IPR expressed in terms of sphere, cylinder, and axis for RCS powers (Fig. 1) and refracted peripheral powers by the lens of BVP -5.76 and base $+2.00$ (Fig. 2).
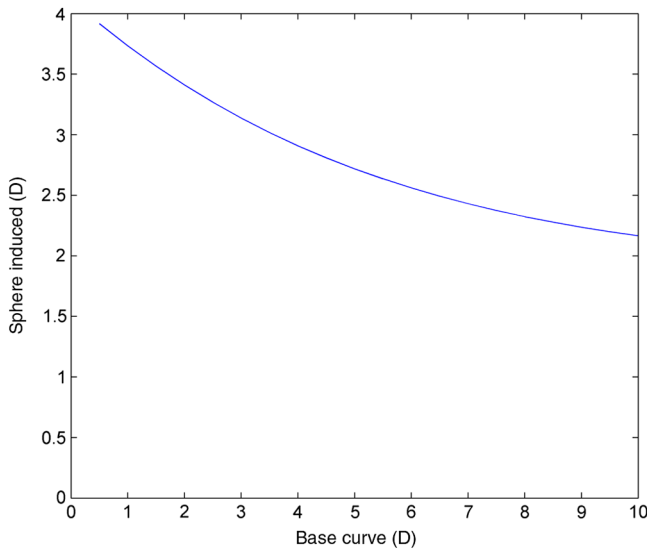
Fig. 5 Peripheral refracted surfaces for M (a), J_0 (b), and J_{45} (c), and contours for M (d), J_0 (e), and J_{45} (f) for a spherical ophthalmic lens with BVP of -5.76D and base curve $+8.00$. The other parameters are those described in the text.

Fig. 6 IPR expressed in terms of sphere, cylinder, and axis for RCS powers (Fig. 1) and refracted peripheral powers by the lens of BVP -5.76 and base $+8.00$ (Fig. 3).

Fig. 7 Representation of induced sphere in front of base curve of a lens of BVP −5.76D, index 1.597, and thickness 1.6. An increase in the power of the base curve produces a decrease in the induced sphere. The RCS is that considered in Fig. 1.

regarding IPR has been set to a base curve of +2.00D in Fig. 4 and to +8.00 in Fig. 6. If different values of asphericity are set at the concave surface keeping the RCS defined as in Fig. 1, the effect of aspherization at the concave surface on peripheral refraction may be observed, especially when the base curve is steeper.

The hypothesis that a peripheral hyperopic refractive error is a risk factor for the development of myopia implies that the peripheral retina is sensitive to defocus and its sign and can generate a signal to control ocular growth. The ability of the peripheral visual system to detect focus change has been evaluated by studies of both depth of focus[37,38] and accommodation.[39,40] There is good evidence to suggest that accommodation can be induced by stimuli lying several degrees outside the central fovea, although with progressively reduced efficiency and eccentricity, and there is some evidence that peripheral accommodation may be less effective

in myopes than emmetropes. Accommodation studies suggest that stimuli falling on the peripheral retina can alter the accommodation response of the eye and, in the presence of an axial accommodation target, can affect the response to the latter.

It is widely accepted that undercorrection of myopia produces a greater degree of myopic progression than full correction.[41,42] A recent study has reported the effect of over-, under-, and full correction on peripheral refraction using contact lenses.[43] It would be expected that contact lenses would change the peripheral refraction profile in a myopic or hyperopic direction compared with full correction. However, the shift between full and overcorrection was slightly less than full and undercorrection in both low and moderate myopes. This is probably due to accommodation with overcorrection resulting in a slightly more myopic refraction measurement. The approach proposed in this paper easily obtains theoretical peripheral refraction profiles when over- or undercorrection is proposed by ophthalmic lenses. These profiles can be used as a reference when experimental values are obtained and accommodation is occurring.

Next figures show peripheral refraction profiles for the RCS proposed when the central refractive error is over- (Fig. 9) or undercorrected (Fig. 10) 1.00D, and the base curve of the lens is maintained to that in Fig. 2. As expected, with overcorrection, a more hyperopic peripheral refraction profile is obtained with respect to full correction and a less hyperopic peripheral refraction profile is obtained with undercorrection, although no changes are observed in the cylinder.

To extend the method to other types of refractive errors, data obtained for emmetropes from the same study[29] are used to model an RCS for an emmetropic eye. Figure 11 shows the RCS for this case. It can be observed that the M value for the RCS changes less than one diopter from the foveal refraction, with areas with light hyperopic peripheral refraction and others with light myopic peripheral refraction. For completeness, the values we have used for the calculation of the RCS are detailed in Table 2.

This RCS is used as a reference to calculate IPR. We consider a lens with BVP of −0.32D (the mean foveal value for


(a)

(b)
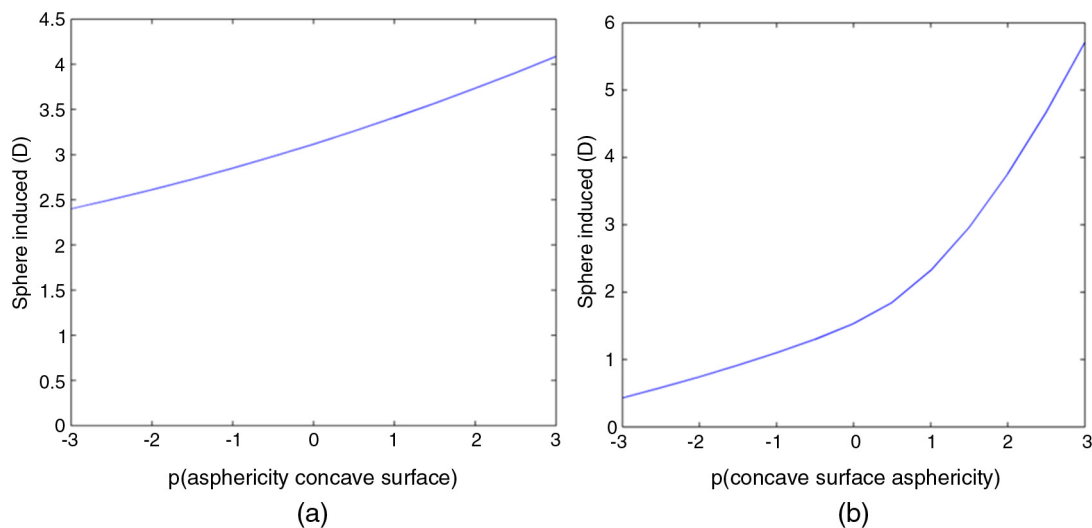
Fig. 8 Effect on sphere induced when asphericity for concave surface is changed, when base curve is +2.00 (a) and when base curve is +8.00 (b). The RCS is that represented in Fig. 1.
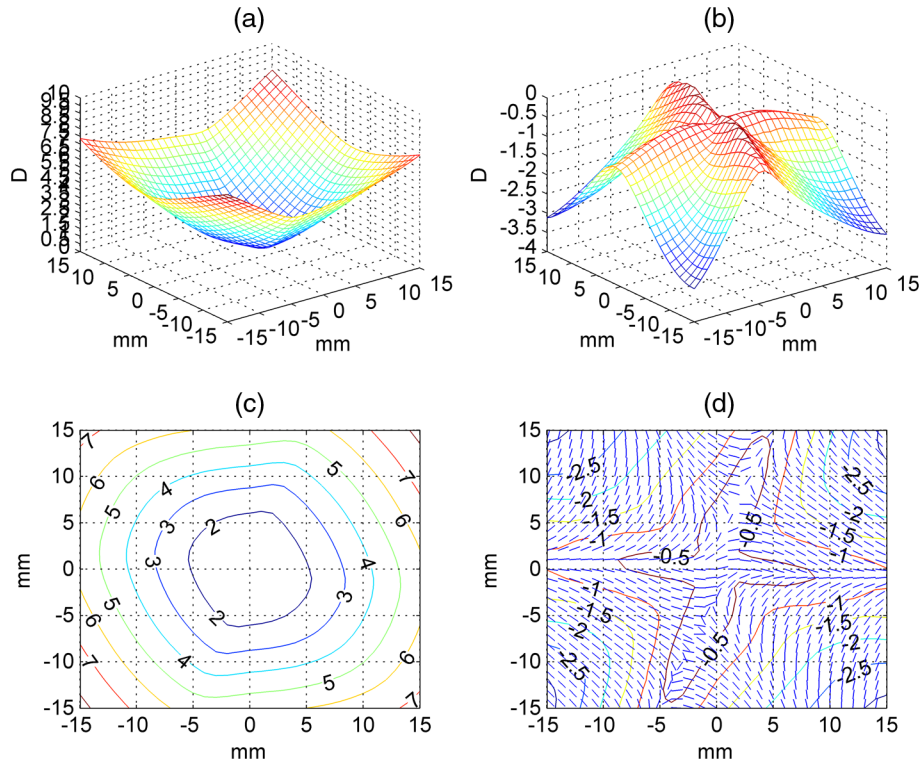
Fig. 9 Overcorrection. IPR expressed in terms of sphere, cylinder, and axis for RCS powers (Fig. 1) and refracted peripheral powers by a lens of BVP −6.76 with the same parameters of the lens in Fig. 2.
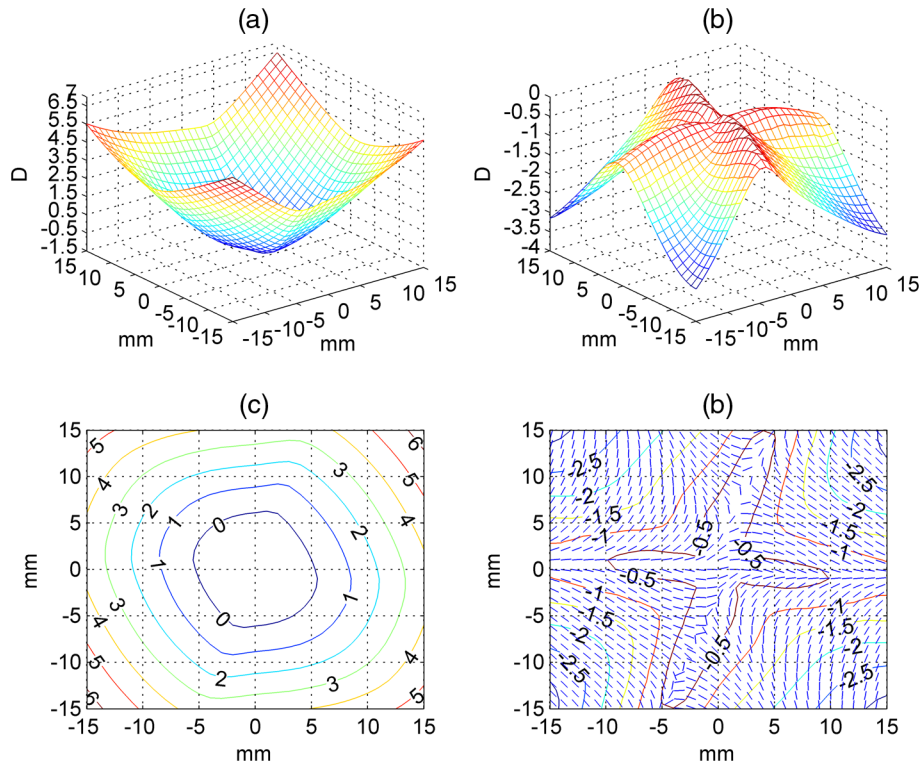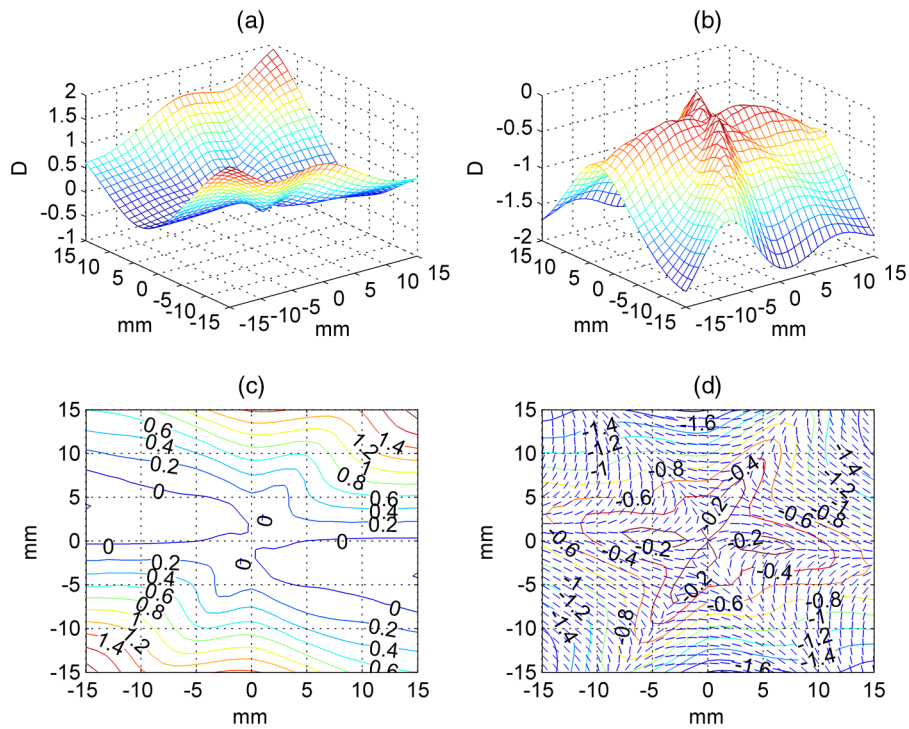
Fig. 10 Undercorrection. IPR expressed in terms of sphere, cylinder, and axis for RCS powers (Fig. 1) and refracted peripheral powers by a lens of BVP −4.76 with the same parameters of the lens in Fig. 2.
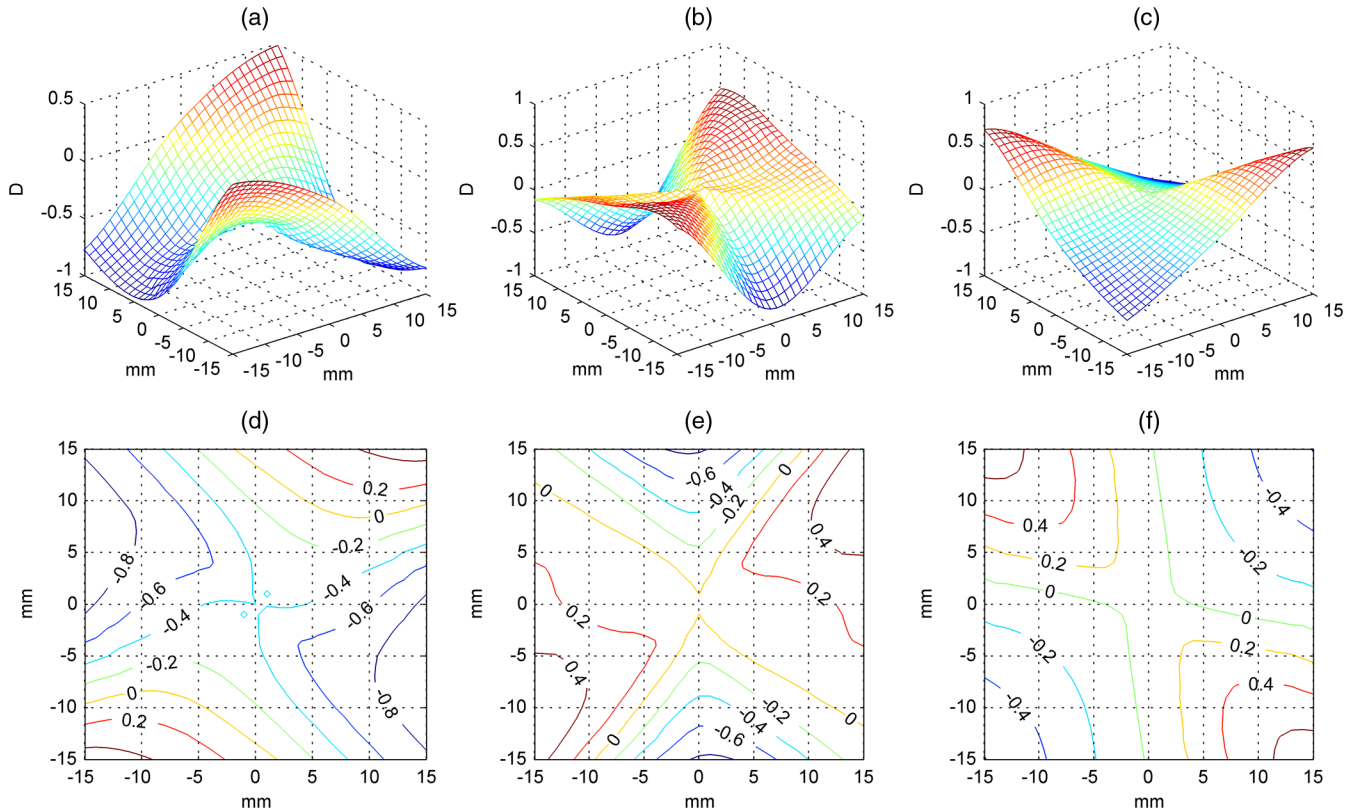
Fig. 11 RCS for M, J_0, and J_{45} using the data from Table 2. Top, surfaces for M (a), J_0 (b), and J_{45} (c); bottom, contour values for the respective surfaces: M (d), J_0 (e), and J_{45} (f).

**Table 2** Mean values of peripheral refraction for emmetropic eyes used to build the RCS.[21]

|	Temporal retina			Central	Nasal retina		
	−30 deg	−20 deg	−10 deg	0	+10 deg	+20 deg	+30 deg
				Horizontal meridian			
M	−0.18 ± 1.34	−0.26 ± 0.95	−0.34 ± 0.62	−0.32 ± 0.44	−0.34 ± 0.63	0.09 ± 0.74	0.40 ± 01.12
J_0	−0.59 ± 0.79	−0.23 ± 0.38	−0.06 ± 0.23	0.06 ± 0.16	−0.03 ± 0.34	−0.06 ± 0.41	−0.09 ± 0.75
J_{45}	0.10 ± 0.65	−0.04 ± 0.52	−0.08 ± 0.18	0.05 ± 0.13	0.05 ± 0.31	0.04 ± 0.31	−0.09 ± 0.46
				Vertical meridian			
M	0.63 ± 1.45	−0.40 ± 1.03	−0.54 ± 0.79	−0.32 ± 0.44	−0.49 ± 0.61	−0.58 ± 0.62	−0.99 ± 1.15
J_0	−0.02 ± 0.98	0.24 ± 0.48	0.30 ± 0.29	0.06 ± 0.16	0.15 ± 0.24	0.32 ± 0.40	0.97 ± 0.87
J_{45}	−0.10 ± 0.32	−0.03 ± 0.33	0.02 ± 0.21	0.05 ± 0.13	0.10 ± 0.24	0.19 ± 0.46	0.23 ± 0.54
				Oblique meridian: superior temporal-inferior nasal			
M	−0.76 ± 1.45	−0.58 ± 0.90	−0.57 ± 0.68	−0.32 ± 0.44	−0.36 ± 0.87	−0.31 ± 0.77	0.13 ± 1.06
J_0	0.01 ± 0.66	0.04 ± 0.33	0.01 ± 0.22	0.06 ± 0.16	0.26 ± 0.37	0.34 ± 0.34	0.19 ± 0.62
J_{45}	0.44 ± 1.40	−0.22 ± 0.50	0.11 ± 0.30	0.05 ± 0.13	0.04 ± 0.26	0.03 ± 0.49	−0.11 ± 0.61
				Oblique meridian: superior nasal-inferior temporal			
M	−0.10 ± 0.97	−0.18 ± 0.87	−0.39 ± 0.77	−0.32 ± 0.44	−0.46 ± 1.07	−0.50 ± 1.32	−0.09 ± 1.60
J_0	0.34 ± 0.40	0.21 ± 0.27	0.14 ± 0.23	0.06 ± 0.16	0.01 ± 0.24	0.05 ± 0.46	−0.17 ± 0.60
J_{45}	−0.26 ± 0.47	−0.06 ± 0.29	−0.01 ± 0.23	0.05 ± 0.13	0.00 ± 0.17	−0.05 ± 0.35	−0.11 ± 0.55

Fig. 12 IPR expressed in terms of sphere, cylinder, and axis for RCS powers (Fig. 11) and refracted peripheral powers by a lens of BVP −0.32 with parameters described in the text.

emmetropic eyes in the study) to consider the case where the refractive error is fully corrected (Fig. 12). Overcorrected and undercorrected situations are shown in Figs. 13 and 14, respectively, with lenses of −1.32D and +0.68D. These lenses have a base curve of +2.00D, index of

refraction of 1.597, thickness of 3 mm, and are situated 12 mm in front of the anterior corneal surface. The feasibility of the method for the calculation of the induced peripheral refraction for different central refractive conditions, thus, becomes demonstrated.
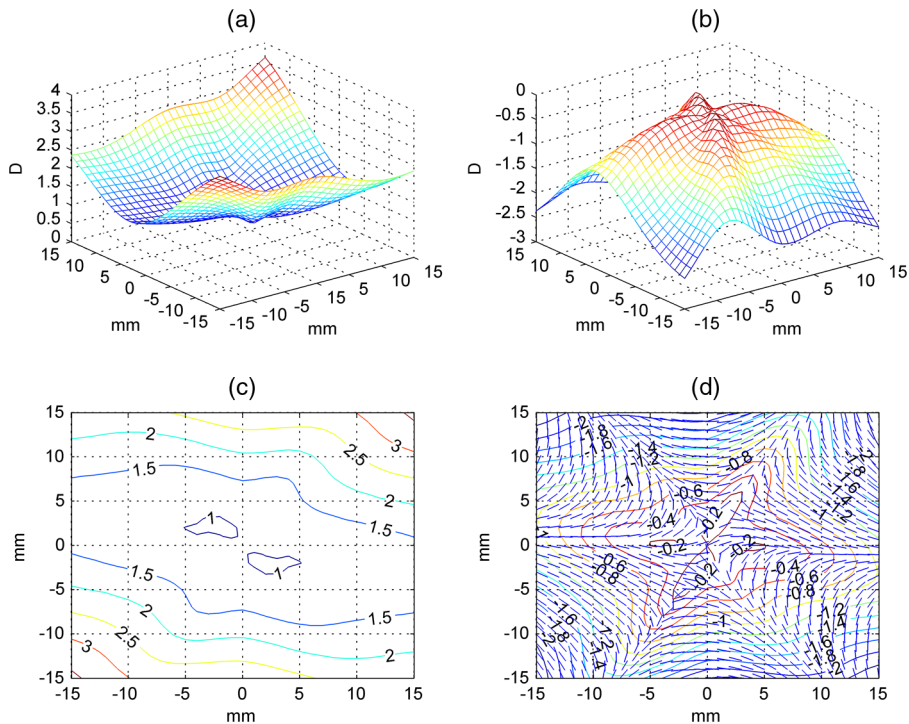
Fig. 13 Overcorrection. IPR expressed in terms of sphere, cylinder, and axis for RCS powers (Fig. 11) and refracted peripheral powers by a lens of BVP −1.32 with parameters described in the text.
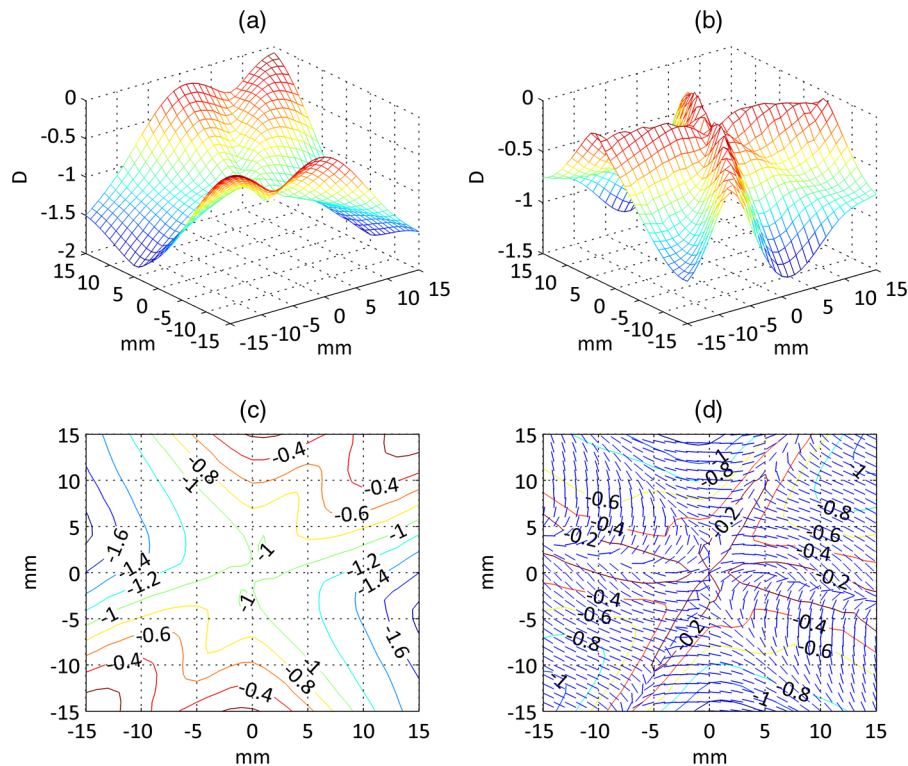
Fig. 14 Undercorrection. IPR expressed in terms of sphere, cylinder, and axis for RCS powers (Fig. 11) and refracted peripheral powers by a lens of BVP +0.68 with parameters described in the text.

4 Conclusion

This work provides a reliable methodology for the calculation of a personalized IPR by an ophthalmic lens on the retinal surface around the fovea. The procedure is based on the general principles of GRT and is, thus, immediately applicable to conventional ophthalmic lens design procedures. To properly calculate peripheral refraction, rays are traced through the nodal point of the eye, and the peripheral refracted error surfaces that are calculated are compared with the RCS, an imaginary surface describing the peripheral refractive error of the patient. Such a surface may be either modeled or measured. The combination of both surfaces enables the calculation of the IPR for a given lens and patient. The effects on IPR of the modification of the curvature and the asphericity of one surface of a lens have been explored as examples of the potential of the method, but the methodology is fully applicable to other lens shapes, including freeform surfaces. The effects of over- and undercorrection of the central refractive error have also been explored and could be used as a reference for experimental measures where there is accommodation.

The methodology proposed studies the effects of lens performance or lens power on a personalized IPR pattern, when the eye is looking in the primary direction of gaze, that is, through the optical center of a nontilted lens. The method opens the door to the evaluation of both peripheral and foveal vision in all directions of gaze and, thus, to the optimization of lenses for both vision conditions. To the best of our knowledge, this is the first proposal involving classical GRT applied to the evaluation of IPR, which can contribute significant advantages in ophthalmic lens designs for children and teenagers, where a free-form approach may be introduced depending on the RCS shape measured. Once the IPR calculation method has been introduced, it becomes possible to design lenses where trade-offs between foveal and peripheral effects are set, so foveal vision is preserved while undesired progression of myopia due to peripheral refraction may be minimized. At the same time, the theoretical values of IPR when over- and undercorrection of the refractive central error are proposed can help us to understand the effects of accommodation on peripheral refraction and its link to the progression of myopia.

References

1. J. Hoogerheide, F. Rempt, and W. P. Hoogenboom, "Acquired myopia in young pilots," *Ophthalmologica* **163**(4), 209–215 (1971).
2. D. O. Mutti et al., "Refractive error, axial length, and relative peripheral refractive error before and after the onset of myopia," *Invest. Ophthalmol. Vis. Sci.* **48**(6), 2510–2519 (2007).
3. M. Millodot, "Effect of ametropia on peripheral refraction," *Am. J. Optom. Physiol. Opt.* **58**(9), 691–695 (1981)
4. J. Wallman and J. Winawer, "Homeostasis of eye growth and the question of myopia," *Neuron* **43**(4), 447–468 (2004).
5. E. L. Smith et al., "Peripheral vision can influence eye growth and refractive development in infant monkeys," *Invest. Ophthalmol. Vis. Sci.* **46**(11), 3965–3972 (2005).
6. C. C. A. Sng et al., "Change in peripheral refraction over time in Singapore Chinese children," *Invest. Ophthalmol. Vis. Sci.* **52**(11), 7880–7887 (2011).
7. D. O. Mutti et al., "Relative peripheral refractive error and the risk of onset and progression of myopia in children," *Invest. Ophthalmol. Vis. Sci.* **52**(1), 199–205 (2011).
8. H. Radhakrishnan et al., "Peripheral refractive changes associated with myopia progression," *Invest. Ophthalmol. Vis. Sci.* **54**(2), 1573–1581 (2013).

9. L. N. Thibos et al., "Spherical aberration and the sign of defocus," *Optom. Vis. Sci.* **90**(11), 1284–1291 (2013).
10. C. Fedtke, K. Ehrmann, and B. A. Holden, "A review of peripheral refraction techniques," *Optom. Vis. Sci.* **86**(5), 429–446 (2009).
11. J. Tabernero and F. Schaeffel, "More irregular eye shape in low myopia than in emmetropia," *Invest. Ophthalmol. Vis. Sci.* **50**(9), 4516–4522 (2009).
12. B. Jaeken and P. Artal, "Optical quality of emmetropic and myopic eyes in the periphery measured with high-angular resolution," *Invest. Ophthalmol. Vis. Sci.* **53**(7), 3405–3413 (2012).
13. X. Wei and L. Thibos, "Design and validation of a scanning Shack Hartmann aberrometer for measurements of the eye over a wide field of view," *Opt. Express* **18**(11), 34–43 (2010).
14. C. Fedtke et al., "The BHVI-EyeMapper: peripheral refraction and aberration profiles," *Optom. Vis. Sci.* **91**(10), 1199–1207 (2014).
15. D. A. Atchison, N. Pritchard, and K. L. Schmid, "Peripheral refraction along the horizontal and vertical visual fields in myopia," *Vis. Res.* **46**(8–9), 1450–1458 (2006).
16. A. Seidemann et al., "Peripheral refractive errors in myopic, emmetropic, and hyperopic young subjects," *J. Opt. Soc. Am. A* **19**(12), 2363–2373 (2002).
17. X. Chen et al., "Characteristics of peripheral refractive errors of myopic and non-myopic Chinese eyes," *Vis. Res.* **50**(1), 31–35 (2010).
18. D. O. Mutti et al., "Peripheral refraction and ocular shape in children," *Invest. Ophthalmol. Vis. Sci.* **41**(5), 1022–1030 (2000).
19. D. A. Atchison et al., "Shape of the retinal surface in emmetropia and myopia," *Invest. Ophthalmol. Vis. Sci.* **46**(8), 2698–2707 (2005).
20. E. L. Smith et al., "Methods and apparatuses of altering curvature of field and positions of peripheral off-axis focal positions," U.S. Patent 7025460B2 (2006).
21. P. Sankaridurg et al., "Spectacle lenses designed to reduce progression of myopia: 12-month results," *Optom. Vis. Sci.* **87**(9), 631–641 (2010).
22. A. Ho et al., "Method and apparatus for controlling peripheral image position for reducing progression of myopia," U.S. Patent 20070159601 A1 (2007).
23. C. H. To, S. Y. Lam, and S. K. Wan, "Method of optical treatment," U.S. Patent 7506983 B2 (2009).
24. J. Tabernero et al., "Effects of myopic spectacle correction and radial refractive gradient spectacles on peripheral refraction," *Vis. Res.* **49**(17), 2176–2186 (2009).
25. Z. Lin et al., "Peripheral defocus with single-vision spectacle lenses in myopic children," *Optom. Vis. Sci.* **87**(1), 4–9 (2010).
26. D. A. Atchison, "Third-order theory of spectacle lenses applied to correction of peripheral refractive errors," *Optom. Vis. Sci.* **88**(2), 227–233 (2011).
27. P. Rojo et al., "Numerical implementation of generalized Coddington equations for ophthalmic lens design," *J. Mod. Opt.* **30**, 1–11 (2011).
28. L. N. Thibos, W. Wheeler, and D. Horner, "Power vectors: an application of Fourier analysis to the description and statistical analysis of refractive error," *Optom. Vis. Sci.* **74**(6), 367–375 (1997).
29. A. Ehsaei et al., "Cross-sectional sample of peripheral refraction in four meridians in myopes and emmetropes," *Invest. Ophthalmol. Vis. Sci.* **52**(10), 7574–7585 (2011).
30. T. Yamaguchi et al., "Peripheral optical quality and myopia progression in children," *Graefes Arch. Clin. Exp. Ophthalmol.* **251**(10), 2451–2461 (2013).
31. A. Mathur, D. A. Atchison, and W. N. Charman, "Myopia and peripheral ocular aberrations," *J. Vis.* **9**(10), 1–12 (2009).
32. O. N. Stavroudis, *The Optics of Rays, Wavefronts, and Caustics*, Academic Press, New York (1972).
33. O. N. Stavroudis, "Simpler derivation of the formulas for generalized ray tracing," *J. Opt. Soc. Am.* **66**(12), 1330–1333 (1976).
34. D. Atchison and G. Smith, *Optics of the Human Eye*, Butterworth-Heinemann, Oxford (2000).
35. L. Bores, *Refractive Eye Surgery*, 2nd ed., Blakwell, Boston (2001).
36. W. F. Harris, "Nodes and nodal points and lines in eyes and other optical systems," *Ophthalmic Physiol. Opt.* **30**(1), 24–42 (2010).
37. B. Wang and K. J. Ciuffreda, "Depth-of-focus of the human eye in the near retinal periphery," *Vis. Res.* **44**(11):1115–1125 (2004).
38. B. Wang and K. J. Ciuffredda, "Blur discrimination of the human eye in the near retinal periphery," *Optom. Vis. Sci.* **82**(1), 52–58 (2005).
39. A. Hartwig, W. N. Charman, and H. Radhakrishnan, "Accommodative response to peripheral stimuli in myopes and emmetropes," *Ophthalmic Physiol. Opt.* **31**(1), 91–99 (2011).
40. Y. C. Gu and G. E. Legge, "Accommodation to stimuli in peripheral vision," *J. Opt. Soc. Am. A* **4**(8), 1681–1687 (1987).
41. J. Cooper, E. Schulman, and N. Jamal, "Current status on the development and treatment of myopia," *Optometry* **83**(5), 179–199 (2012).
42. B. Vasudevan et al., "Under-correction of human myopia—is it myopigenic? A retrospective analysis of clinical refraction data," *J. Optom.* **7**(3), 147–152 (2014).
43. P. F. Y. Kang et al., "Effect of single vision soft contact lenses on peripheral refraction," *Optom. Vis. Sci.* **89**(7), 1014–1021 (2012).

Pilar Rojo has been an assistant professor at the Facultat d'Òptica i Optometria de Terrrassa. She received her MS degree in optometry and vision science from the same university in 2010, and she is currently working on her PhD. Her interest in myopia led her to develop her PhD program in ophthalmic lens design related to myopia progression. She has also been working at Industrias de Óptica Prats for the past year.

Santiago Royo received his PhD degree in applied optics from Universitat Politècnica de Catalunya (UPC-BarcelonaTech) in 1999. He is currently associate professor at UPC and director of the Center for Sensor, Instruments and System Development (CD6), a research and innovation center in Optical Engineering in Terrassa, where seven spin-off and four start-up companies have been created. For twenty years he has participated and led research projects in optical metrology and engineering, leading him to publish over 50 full-text publications and 10 patents, five of them licensed. He is cofounder of two photonics-based spin-off companies.

Jesus Caum received his PhD degree in optical engineering from Universitat Politècnica de Catalunya (UPC-BarcelonaTech) in 2009. He is currently associate professor at UPC and researcher at the Center for Sensor, Instruments and System Development (CD6), a research and innovation center in Optical Engineering in Terrassa, where seven spin-off and four start-up companies have been created.

Biographies of the other authors are not available.